Thermolytic reverse electrodialysis heat engine: model development, integration and performance analysis

Thermolytic Reverse Electrodialysis Heat Engine: model development, integration and performance analysis

F. Giacalone[a], F. Vassallo[a], L. Griffin[a,b], M.C. Ferrari[b], G. Micale[a], F. Scargiali[a]*, A. Tamburini[a], A.Cipollina[a]

[a]Dipartimento dell'Innovazione Industriale e Digitale (DIID), Università degli Studi di Palermo (UNIPA), viale delle Scienze Ed.6, 90128 Palermo, Italy.

[b]School of Engineering, Institute for Materials and Processes, The University of Edinburgh, The King's Buildings, Edinburgh EH9 3JL, UK

*e–mail: francesca.scargiali@unipa.it,

ABSTRACT

Salinity gradient heat engines represent an innovative and promising way to convert low-grade heat into electricity by employing salinity gradient technology in a closed-loop configuration. Among the aqueous solutions which can be used as working fluid, ammonium bicarbonate-water solutions appear very promising due to their capability to decompose at low temperature. In this work, an experimentally validated model for a reverse electrodialysis heat engine fed with ammonium bicarbonate-water solutions was developed. The model consists of two validated sub-models purposely integrated, one for the reverse electrodialysis unit and the other for the stripping/absorption regeneration unit. The impact of using current commercial membranes and future enhanced membranes on the efficiency of the system was evaluated, along with the effect of operating and design parameters through sensitivity analyses. Results indicated that exergy efficiency up to 8.5% may be obtained by considering enhanced future membranes and multi-column regeneration units.

KEYWORDS

Thermolytic salts, Salinity Gradient Heat Engine, Regeneration unit, Reverse Electrodialysis, Ammonium Bicarbonate solutions, Waste Heat Recovery.

1 INTRODUCTION

The increasing demand of energy due to population and industrial growth is an open issue nowadays, while increasing attention is paid to the sustainable production of energy. In this scenario of opposing challenges, interest towards non-conventional or under-used resources is rapidly increasing. Low-grade heat coming from geothermal sources, sun or industrial activities is a resource being as abundant as under-used, because no technology has been proposed so far to convert efficiently such heat into electricity [1]. The potential availability of waste heat in the EU industrial sector has been estimated at about 304.13 TWh/year, mainly represented by waste heat at temperatures in the range 100-200 °C (40% of the total) [2].

Salinity gradient power heat engines (SGP HEs) have been recently proposed as a viable process to convert low-grade heat into electricity [3]. A SGP HE system consists of two main units: (i) a power generation unit based on salinity gradient power process, where the concentration difference between two salt solutions is exploited to produce electricity, and (ii) a regeneration unit where low-grade heat is used to restore the original concentration values of the solutions exiting from the power generation unit. The restoring of the two solutions can be achieved by means of different strategies, e.g. (i) solvent extraction and (ii) salt extraction [1]. In solvent extraction, the salt exchanged within the power unit is rebalanced by adding a part of the exhausted dilute stream to the exhausted concentrate stream. Then, the resulting solution is fed to the regeneration unit where the solvent is recovered by a thermal separation process (e.g. multi-effect distillation, membrane distillation) and transferred to the dilute solution.

In salt extraction, the exhausted dilute solution is fed to the regenerative unit where salt is recovered by using low-grade heat and transferred again to the concentrate solution. Rebalancing of the solvent is eventually carried-out to restore the solvent amount in the two streams.

The concept of SGP HE was proposed for the first time by Loeb more than forty years ago, for both pressure retarded osmosis (PRO) [4] and reverse electrodialysis (RED) [5] heat engines. Only in recent years, the growing improvement and the decreasing cost of the membranes used in SGP technologies are boosting research interest on this topic.

Compared to open loop SGP technologies, SGP HEs give the great advantage of allowing artificial streams in a closed circuit along with the adoption of any solute-solvent couple. This advantage avoids the geographical constraint of limited availability of streams at different salinity and, more importantly, allows to achieve higher performances as the salinity gradient can be suitably chosen and tuned.

Several works have been already devoted to different SGP HE configurations. In particular, both solvent and salt extraction strategies have been studied. As concerns the solvent extraction strategy, some works investigated the performance of SGP HEs with different regeneration technologies for the case of sodium chloride (NaCl) - water solutions. Lin et al. [6] carried out a theoretical study on a heat engine, in which PRO (an osmotic heat engine, OHE) was coupled with a membrane distillation (MD) regeneration unit. Long et al. [7] performed a parametric study on a hybrid RED-MD system. The results showed, in best conditions, a maximum exergy efficiency of about 10%. Similarly, Micari et al. [8] performed a theoretical analysis for the design of a RED-MD prototype considering the behaviour of real units and providing perspectives. An integrated system can provide an exergy efficiency equal to 2.3%, while considering technological improvements on both units, an exergy efficiency of 16.5% can be achieved.

Recently, other studies reported theoretical analysis concerning the performance of a heat engine coupling a RED unit with a multi effect distillation system (MED). In particular, Hu et al. [9] reported a maximum exergy efficiency of about 5%, coupling a RED unit with a MED of 10 effects fed with low-grade heat at 95 °C. Palenzuela et al. [10] investigated the impact of membrane properties and operating conditions on the integrated system. They reported an exergy efficiency around 7% for the case of real membranes using low-grade heat at 100°C, and up to almost 31% for the case of ideal membranes.

Other authors studied the impact of different solute-solvent couples. For instance, Shaulsky et al. [11] proposed an OHE fed by lithium chloride (LiCl) - methanol solutions. Marino et al. [12] proposed an electrochemical cell coupled to a distiller using zinc chloride ($ZnCl_2$) - water solutions as working solution. Hickenbottom et al. [13] experimentally investigated the impact of using different salt solutions as possible working fluid of a PRO-MD HE. Their findings indicate calcium chloride as the most promising salt for both PRO and MD processes. Carati et al. [14] presented a theoretical analysis on SGP HE, focusing on the effect of different salt-water solutions, namely NaCl, $ZnCl_2$ and sodium hydroxide (NaOH) water solutions, on the performance of a unit constituted of a distiller and an ideal SGP unit. Similarly, Giacalone et al. [15] performed a theoretical analysis concerning the influence of different salt-water solutions, namely NaCl, LiCl, potassium chloride (KCl), potassium acetate (KCH_3CO_2), caesium acetate ($CsCH_3CO_2$) and sodium acetate ($NaCH_3CO_2$) water solutions, on the performance of SGP HEs consisting of single and multi-stage regeneration units. Micari et al. [16] experimentally investigated the performance of a RED unit fed by aqueous solutions of binary salt mixtures.

Concerning the salt extraction strategy, the use of aqueous solutions of thermolytic salts has been considered so far as one of the most promising solvent-solute couples. Thermolytic salts

95 have the capability of decomposing into gaseous compounds at the low temperatures at which
96 waste heat is available (60-100°C). Thus, the thermolytic salt of the dilute solution is
97 decomposed into gaseous compounds, subsequently it is adsorbed into the concentrate solution
98 (salt extraction strategy). Ammonium bicarbonate (NH_4HCO_3) is the most commonly used
99 thermolytic salts in such applications as it is able to decompose into carbon dioxide and
100 ammonia above 50-60°C [4]. About ten years ago, McGinnis et al. [17] proposed an OHE where
101 PRO is coupled with a distillation column fed with NH_4HCO_3 solutions. They found that the
102 high thermal energy consumption affects the global energetic efficiency. Similarly, Luo et al.
103 [18] and Cusick et al. [19] proposed a RED unit and a microbial RED unit, respectively, fed
104 with NH_4HCO_3 solution and coupled to a distillation column.
105 In recent years, several researchers have focused their attention on the performance of RED
106 units fed by NH_4HCO_3 aqueous solutions. In particular, Kwon et al. [20] presented an
107 experimental analysis, reporting a maximum power density (1.54 $W/m^2_{cell\ pair}$), doubling that
108 achieved by Luo et al. [18]. Similarly, Bevacqua et al. [21] presented an experimental
109 investigation aimed to maximize the performance of a laboratory RED unit fed by NH_4HCO_3,
110 recording the highest power density achieved so far in RED units fed by aqueous solutions of
111 NH_4HCO_3 (i.e., 2.42 $W/m^2_{cell\ pair}$). In 2017, Kim et al. [22] proposed a validated model to predict
112 the performance of a RED unit fed by NH_4HCO_3 solutions.
113 A first preliminary attempt to perform an accurate analysis of the whole heat engine including
114 also the regeneration step was performed for the first time by Bevacqua et al. [23], who carried
115 out a modelling analysis on a RED HE system operating with aqueous solution of NH_4HCO_3.
116 The proposed HE consists of a RED unit and a thermal regeneration unit including an air
117 stripping column to restore the initial salinity gradient. The highest energy efficiency reported
118 was equal to 22%.

Notwithstanding the growing interest on RED HEs only few theoretical studies have been carried out so far on the whole system. Most of them were focused on the RED unit without analysing the regeneration unit and the integrated system performances.

In a previous work [24], a validated RED model used to perform an exergy analysis of RED units fed with NaCl-water solutions was presented. In the present work, an experimentally validated model of a RED HE (as a whole) fed by thermolytic NH_4HCO_3 solutions (t-RED HE) is presented. The proposed t-RED HE consists of a RED unit coupled to a vapour stripping column for the stripping of the salts, and an absorption process where the gases are reabsorbed. The model comes from the integration of two sub-models: (i) the RED unit model, obtained by upgrading the previous RED model [23]; (ii) the stripping/absorption regeneration units, purposely developed in Aspen plus®. Sensitivity analyses were carried out in order to evaluate the performance of the RED HE as a whole. The effect of operating and design parameters on the thermal and exergy efficiencies of the system was investigated. Furthermore, a perspective analysis is presented assuming enhanced properties of the ionic exchange membranes (IEMs).

2 METHODS

The thermolytic RED HE is composed of two units: (i) a RED unit where power is produced exploiting the salinity gradient between NH_4HCO_3 solutions as the "power generation unit"; (ii) a thermal regeneration unit where low-grade waste heat is used to restore the initial conditions of the two streams exiting the RED unit, as the "regeneration unit". A schematic representation of the entire t-RED HE is reported in Figure 1.

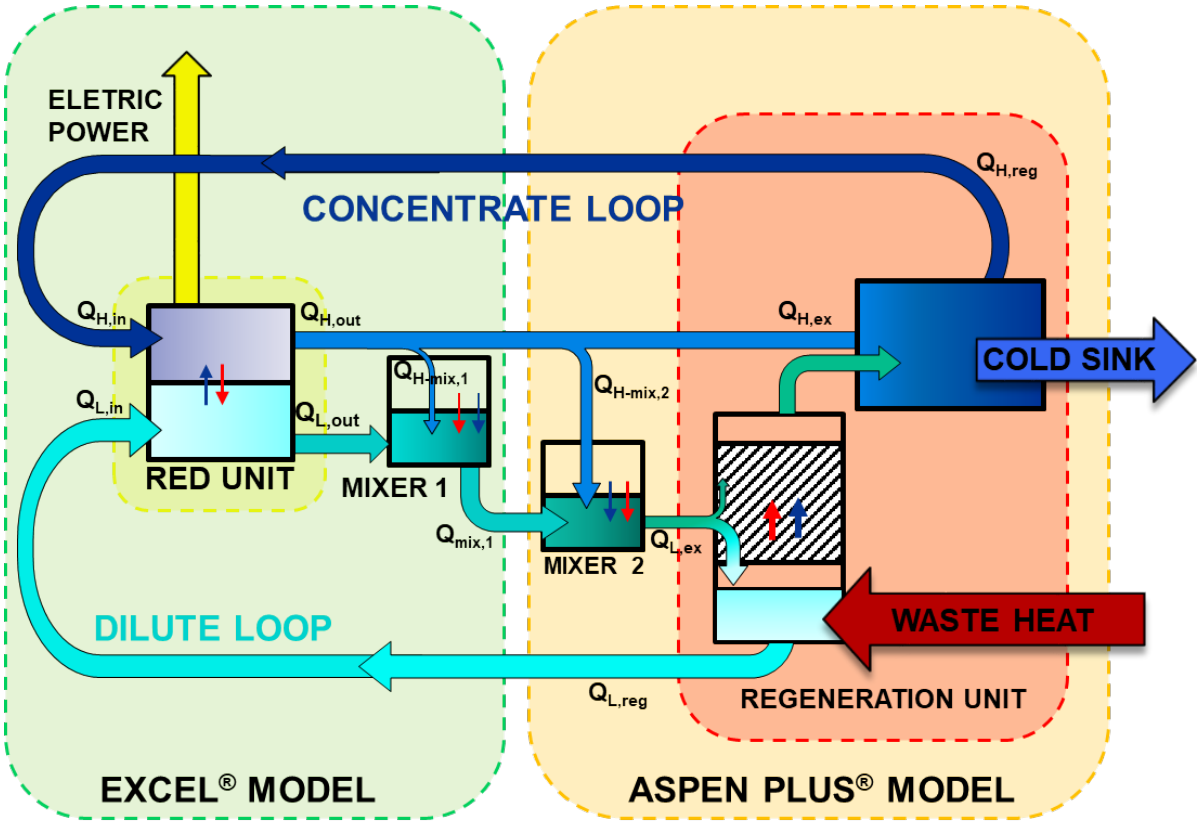

Figure 1 *System scheme used in the exergy analysis. Blue arrows indicate the direction of water fluxes while red arrows indicate the direction of salt fluxes.*

The two NH_4HCO_3 solutions, i.e., the dilute and the concentrate, are pumped to the RED unit to convert their salinity gradient into electricity. During the process, part of the salt content in the concentrate solution is transferred to the dilute solution, while water is transferred from dilute to concentrate due to the osmotic flux. In order to restore the initial conditions of the two streams in the regeneration unit, both salt and water transport have to be promoted in the opposite direction.

After exiting from the RED stack, the dilute solution is mixed with a small amount of the concentrate stream in mixer 1, in order to restore the water content in the dilute stream. Notably, this step is extremely important in order to restore the flow rate of the two streams since the system operates in a closed loop. The second mixer (mixer 2) fulfils a similar task, restoring the amount of water consumed in the stripping process due to the partial vaporization of the

dilute stream. In practical applications, the water-restoring step can be carried out in one mixer only. Here, two different mixers are considered because the two sub-models (i.e., one for the RED unit and one for the regeneration unit) are developed in different software and each of them includes a mixer. The resulting stream from mixer 2 is fed to the vapour stripping column operating in vacuum conditions. Here, the NH_4HCO_3 is decomposed into ammonia and carbon dioxide, which are stripped by means of a vapour stream produced from the partial vaporization of the solution in the reboiler. Low-grade waste heat ($T \leq 100$ °C) is used as an energy source. The stripped gasses are absorbed again into the concentrate solution through a low temperature (25 °C) absorption process. The two regenerated solutions are finally sent back to the stack where their difference in chemical potential is used again to generate electricity.

The whole model consists of two experimentally validated sub-models (Fig. 1):

(i) The RED unit model, including mixer 1, implemented in Excel®;

(ii) The regeneration unit model, including mixer 2, implemented in Aspen plus®.

A description of the model is reported in the following sections.

2.1 Reverse electrodialysis model

The modelling approach is similar to that reported in a previous work [24], where a validated RED model is presented and used to perform an exergy analysis of RED units fed by NaCl-water solutions. In particular, the concentration and flow rate variations along the channels are accounted for by adopting a mono-dimensional approach. The unit, consisting of a given number of cell pairs (i.e., N_{cp}), is discretized in N_k calculation elements along the main flow direction. Each calculation element represents a branch of an equivalent circuit, where passive (i.e., resistances) and active (i.e., generator) elements are present. Full details are reported in [24]. The electric voltage (E_{cell}) produced in the generic k^{th} element of a cell pair is calculated according to the following equation:

$$E_{cell}(k) = 2\alpha_{av}(k)\frac{RT}{zF}\ln\left(\frac{m_H(k)\cdot\gamma_H(k)}{m_L(k)\cdot\gamma_L(k)}\right) \quad (1)$$

where α_{av} is the average membranes permselectivity, γ_H and γ_L are the activity coefficients of the two solutions, m_H and m_L are the solutions molality, z is the z is the valence of the ions, F is the Faraday's constant, R is the universal gas constant and T is the absolute temperature (T= 298 K).

The resistance of the k^{th} element of the cell pair (R_{cell}) is given by the sum of 4 resistances in series:

$$R_{cell}(k) = \left[R_H(k) + R_L(k) + R_{CEM}(k) + R_{AEM}(k)\right]\frac{1}{\Delta x \cdot b} \quad (2)$$

where R_{CEM} and R_{AEM} are the membrane resistances, R_H and R_L the electrical resistances of the solutions flowing in the two channels, Δx is the length of the calculation element and b is the membrane width. Thus, the electric current (i) circulating in the k^{th} branch is computed according to:

$$i(k) = \frac{N_{cp}E_{cell}(k) - (E_{stack} + R_{blank}I_{stack})}{N_{cp}R_{cell}(k)} \quad (3)$$

where E_{stack} is the electric voltage generated by the RED unit and R_{blank} is the resistance of the electrodic compartments, which is negligible for high cell pairs number (e.g. larger than 100 cell pairs). The electric current circulating on the external load (I_{stack}) is the sum of the currents produced in the k^{th} branch (Kirchhoff's junction rule).

$$I_{stack} = \sum_k i(k) \quad (4)$$

The closing equation is obtained by the Ohm's law on the external load (Eq. 5).

$$E_{stack} = R_E \cdot I_{stack} \quad (5)$$

where R_E is the resistance of the external load. The gross power (P_{RED}) and the gross power density (P_d) are calculated as follows:

$$P_{RED} = E_{stack} \cdot I_{stack} \quad (6)$$

$$P_d = \frac{P_{RED}}{N_{cp} A_{cp}} \quad (7)$$

where A_{cp} is the area of a cell pair.

In order to compute the maximum power density ($P_{d,max}$), the value of external load resistance is optimized and is typically set to the same value of the stack internal resistance [8].

The model also considers the water and salt fluxes across the membranes. The model does not account for pressure drops along the channel, thus only gross power and gross power density values are reported. Pressure drops are mainly related to the geometry of stack configuration, and generally account for 10 to 20% . The complete description of the model is reported in [24] for the case on NaCl-water solutions.

In order to account for the variation of the properties of NH_4HCO_3 aqueous solution along the channels, molality-dependent correlations are used. In particular:

(i) the activity and osmotic coefficients of NH_4HCO_3-water solutions are estimated through Pitzer's model [25];

(ii) the densities of the solutions are estimated as a linear function of the molar concentration using literature data to obtain the fitting coefficients [26];

(iii) the salt-solution conductivity is estimated using the Jone and Dole's equation with experimentally fitting parameters [27].

All the relevant equations to estimate the solutions properties and graphical comparisons between fitting equations and experimental literature data are reported in the Appendix.

Membrane resistance and permselectivity variation along the stack are taken into consideration by adopting concentration-dependent correlations provided by the membrane manufacturer, while constant values for water permeability and salt diffusivity were considered (see Table 1 for reference values). In particular, relevant equations for permselectivity versus concentrate

concentration and membrane electrical resistance versus dilute concentration are reported in the following (eqs. 8-9):

$$\alpha_{av} = 0.8924 \cdot C_H^{-0.069} \quad (8)$$

$$R_{IEM,av} = 2.027 \cdot 10^{-4} \cdot C_L^{-0.236} \quad (9)$$

The correlations provide the values of the permselectivity and the electrical resistance ($R_{IEM,av}$) as an average for both the anionic and the cationic exchange membranes.

Simulations were performed considering a RED unit consisting of 1000 cell pairs (cps) with membrane area of 0.5 x 0.5 m^2 and spacers of 0.155 mm. Two different scenarios were analysed: (i) a current scenario in which the RED unit is equipped with current membranes (Fujifilm membranes); (ii) a future scenario in which future membranes with enhanced properties are adopted (see Table 1). The enhancement in the case of future membranes is aimed at decreasing the membrane resistance, the water and salt permeability, while increasing the permselectivity [24]. For the case of NaCl aqueous solutions, the properties of future membranes are not far from those of currently available membranes, as reported in [28] and described in [8].

Table 1. *Current and future membrane properties adopted in the analysis.*

Properties	Current	Future
Permselectivity [%]	85.1(*)	95(**)
Resistance [Ω·m^2]	6.01 10^{-04}(*)	1.50 10^{-04}(*)
Water Permeability [ml/(bar·h·m^2)]	6(**)	1.5(**)
Salt diffusivity [m^2/s]	4.5 10^{-12}(**)	1.13 10^{-12}(**)

(*)*reference concentration of 2 M-0.01 M NH_4HCO_3 water solutions. Property functions of solutions concentration*

(**)*assumed constant in the whole range of concentrations*

The model is closed by trivial global and salt mass balances in mixer 1. These are reported in eqs. 10-11.

244 $$Q_{mix1} \cdot \rho_{mix1} = Q_{L,out} \cdot \rho_{L,out} + Q_{H-mix1} \cdot \rho_{H-mix1} \quad (10)$$

245 $$Q_{mix1} \cdot C_{mix1} = Q_{L,out} \cdot C_{L,out} + Q_{H-mix1} \cdot C_{H,out} \quad (11)$$

246 where Q_i, ρ_i and C_i are the volumetric flowrate, density and concentration of the i^{th} generic
247 stream, respectively. The subscripts *L,out*, *mix1* and H-*mix1* refer to the dilute stream exiting
248 from the RED unit, the stream exiting from the mixer 1 and the part of the concentrate stream
249 exiting from the RED unit added in the mixer, respectively. The $Q_{H\text{-}mix1}$ is evaluated from the
250 water mass balance of the concentrate in the RED unit

251 $$Q_{H-mix1} = \frac{\left[Q_{H,in}(\rho_{H,in} - C_{H,in}MW_s) - Q_{H,out}(\rho_{H,out} - C_{H,out}MW_s)\right]}{\rho_{H,out} - C_{H,out}MW_s} \quad (12)$$

252 where MW_s is the molecular weight of NH_4HCO_3. Subscripts *in* and *out* refer to the inlet and outlet
253 streams in the RED unit.

254 **2.1.1 Reverse electrodialysis model validation**

255 The RED model was validated by comparison with experimental results. Figures 2a and 2b show
256 the trend of experimental and modelling stack voltage (E_{stack}) and power (P_{RED}) for two different
257 salinity gradients (i.e., 0.6 M-0.05 M and 1.6 M-0.05 M) as function of the I_{stack} and the E_{stack},
258 respectively, for a RED unit consisting of 50 cell pairs 0.1 x 0.4 m^2 provided by 0.155 mm spacers
259 and considering solution velocities equal to 0.5 cm/s.
260 Model predictions fit very well with experimental trends, thus indicating the reliability of the
261 model in the range of conditions investigated. The model was further validated considering
262 different salt-water solutions, velocities, concentration and stack geometries, giving always a good
263 agreement [24].

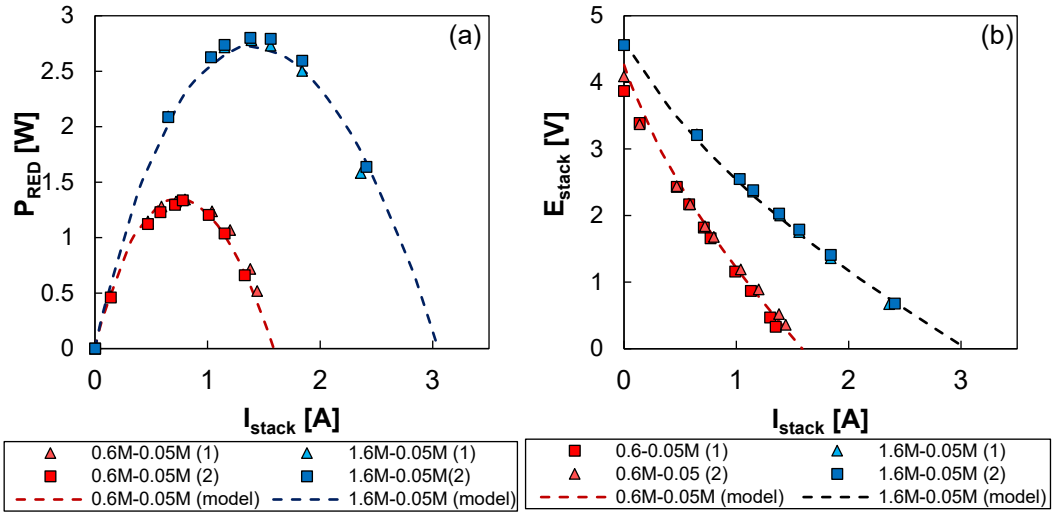

Figure 2. *Power versus electrical current (a) and electrical potential versus current (b) in a RED unit fed by NH_4HCO_3 solutions (0.6 M-0.05 M and 1.6 M-0.05 M) at 0.5 cm/s. RED unit 50 cell pairs 0.1 x 0.4 m^2.*

2.2 Regeneration unit model

The regeneration unit of the thermolytic RED HE was modelled on Aspen plus®. The Aspen flowsheet of the process is reported in Figure 3.

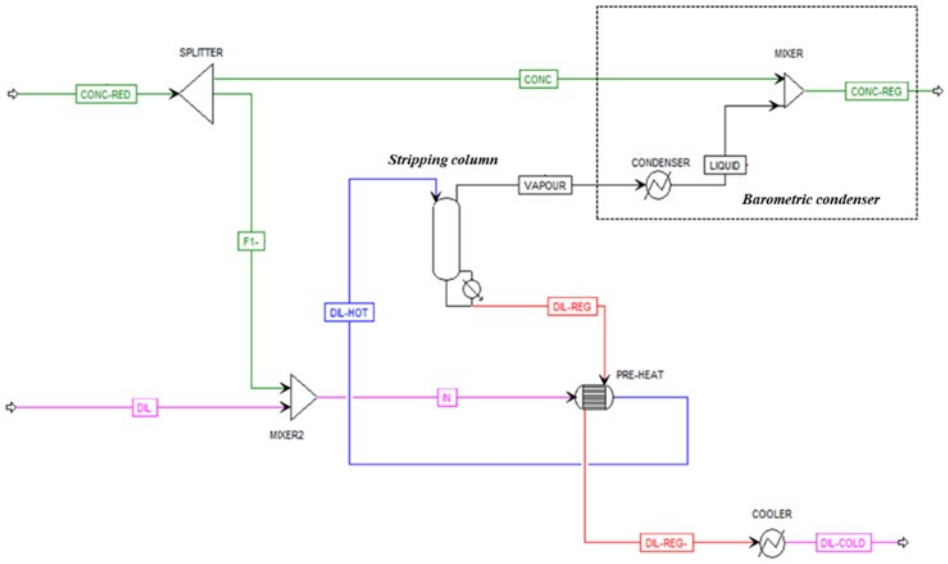

Figure 3. *Aspen flow-sheet of the regeneration process.*

The components and chemical equilibrium reactions involved in NH_4HCO_3-water solutions were described by adopting a multi-model approach. In fact, while the solution properties of

the liquid streams are evaluated adopting the *OLI*® property method, the behaviour of the columns was modelled using the electrolyte non random two liquid Redlich-Kwong (E-NRTL-RK) property method. The behaviour of the stripping column (Stripper) was modelled using a *Rad-Frac* model, which provides rigorous methods for design of multistage separations, such as distillation, absorption, and stripping processes. The model performs simulation, sizing, and rating of tray or packed columns. The stripping column was set in rate-based mode in order to take into account the heat/mass transfer, thermodynamic, hydrodynamic and chemical reaction features. The absorption process was modelled as a mixer and a condenser (Absorber). Mixer 2 is used to restoring the amount of water lost in the dilute solution due to the vaporization within the stripping column.

Concerning the barometric condenser, the cooling stream temperature was assumed equal to 20 °C while the outlet hot stream temperature was set to 25° C. The temperature of the waste heat ($T_{waste\text{-}heat}$) that is used as hot utility in the stripping unit reboiler was assumed equal to 80 °C while the boiling temperature is set to 75 °C.

Setting the chemical and physical properties of the inlet streams and the operating conditions of the main equipment, the simulator computes the properties of outlet streams and evaluates the thermal power consumption (TPC) to achieve a desired separation.

The operating and geometrical properties of the column were set as follows:

- Raschig rings of 15 mm were adopted as packing material;
- a design factor of 70% approach to flooding was chosen to compute the column diameter.
- column height was set equal to 2 m.

A thermal integration heat-exchanger (pre-heater) is used to recover part of the heat stored in the dilute regenerated solution exiting from the reboiler by preheating the solution fed to the vapour stripping column.

299 The concentration and flow rate of the resulting stream exiting from mixer 1 are the input of the
300 Aspen plus® regeneration model.
301 The mass balances for mixer 2 are implemented in the Aspen model flow-sheet. The amount of
302 concentrate solution added to the dilute stream for rebalancing the water content due to the
303 generation of the stripping vapour is evaluated using the *design spec* tool of Aspen plus®. This tool
304 operates as a goal seek with the aim to compute the fraction of the concentrate stream to be added
305 to the dilute in order to balance the water lost in the stripping process. The thermal power required
306 for the separation is thus calculated by using a second *design spec* (operating in parallel to the
307 previous), which adjusts the value of the thermal power in order to get the desired concentration
308 of the regenerated dilute solution.

309 **2.2.1 Stripping unit model validation**

310 The regeneration unit model was validated comparing experimental results of a purposely-made
311 vapour stripping column with Aspen plus® model predictions. The experimental stripping column
312 consists of a structured packed column with a height of 1.6 m and an internal diameter of 5 cm.
313 The packing material is the Koch-Glitsch® FLEXIPAC 700Y. Figure 4 shows the trend of
314 experimental conductivities of the two regenerated solutions as a function of the dilute inlet
315 concentration (ranging from 0.2 M to 0.6 M) and the thermal power consumption (ranging from
316 700 W to 1000 W). The dilute inlet flow rate (i.e., 0.215 l/min) and the regeneration temperature
317 (i.e., between 70-80 °C) were kept constant. A reasonable agreement between experimental
318 results and model predictions was found with a maximum error of about 10% in the case of an
319 inlet concentration equal to 0.6 M .
320

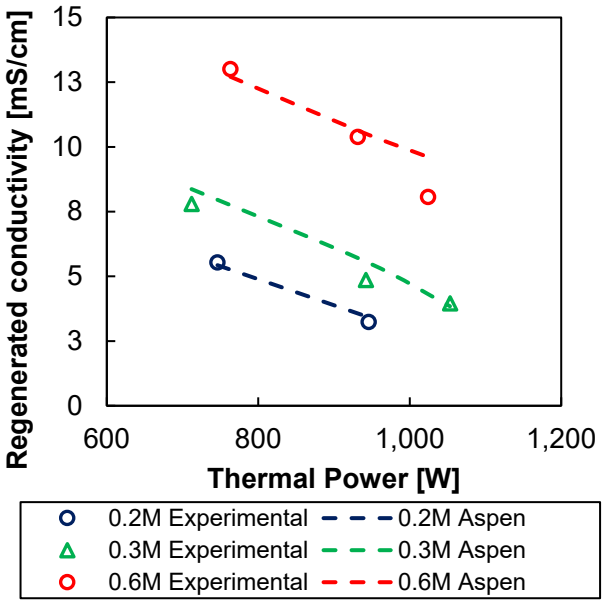

Figure 4. *Comparison of experimental measurements of regenerated solutions conductivity and model predictions as a function of the heat provided to the reboiler and of the inlet molarity of the solutions.*

2.3 Thermal and exergy efficiencies

The thermal efficiency (η_{th}) of the t-RED HE is defined as:

$$\eta_{th} = \frac{P_{RED}}{TPC} \tag{13}$$

The maximum achievable thermal efficiency is equal to the Carnot efficiency (η_C) evaluated at T_{HOT} = 353 K (maximum temperature) and T_{COLD} = 293 K (minimum temperature):

$$\eta_C = 1 - \frac{T_{COLD}}{T_{HOT}} \tag{14}$$

Finally, the exergy efficiency (η_{ex}) of the t-RED HE is the ratio between the energy efficiency and the Carnot efficiency. This parameter has been proposed as the most appropriate to compare different heat engines [29].

$$\eta_{ex} = \frac{\eta_{th}}{\eta_C} \tag{15}$$

It is worth noting that the efficiencies reported in the following do not take into account the electric power consumption due to the pumping of the fluids. The pumping energy is generally strongly affected by RED and regeneration units design. In the present case, the pumping power can be considered as a fraction of the total power output in the range of 10-50%.

The above efficiencies are used along with the power density and the specific thermal consumption as performance parameters in the sensitivity analysis reported in the following.

3 RESULTS AND DISCUSSION

The above mentioned sensitivity analyses were carried out in order to investigate the effect of flowrate and concentration of the two solutions fed into the RED unit on the performance of the integrated system for both current and future scenarios. Finally, the effect of using a multi-stage regeneration unit was analysed.

3.1 Influence of inlet concentration on the system performance

The first sensitivity analyses show the effect of the solution concentration on the main performance parameters of the t-RED HE considering a RED unit consisting of 1000 cell pairs 0.5x0.5 m^2. For the first analysis, the inlet velocity of the two solutions within the spacer-filled channels was set to 1cm/s (i.e., typical value in RED operations).

The influence of the RED inlet concentration on $P_{d,max}$, is reported in Figure 5. As expected, the higher the salinity gradient between the two solutions, the higher the power density obtainable from the unit. As a matter of fact, when long stacks or large residence times are considered as in the present case, the detrimental effect due to the dilute solution resistance becomes less important. Conversely, if laboratory units (i.e., short stacks) or low residence times for the dilute solutions are considered, then the dilute solution resistance is the controlling factor affecting the power density. In the case of current membranes, the highest $P_{d,max}$ is equal to 2 W/m^2 while

in the case of future membranes it is equal to 4.25 W/m^2. The doubling in power density shifting from current to future membrane is due to the reduction of the irreversible phenomena occurring in the RED unit and responsible for the reduction of the available salinity gradient [24].

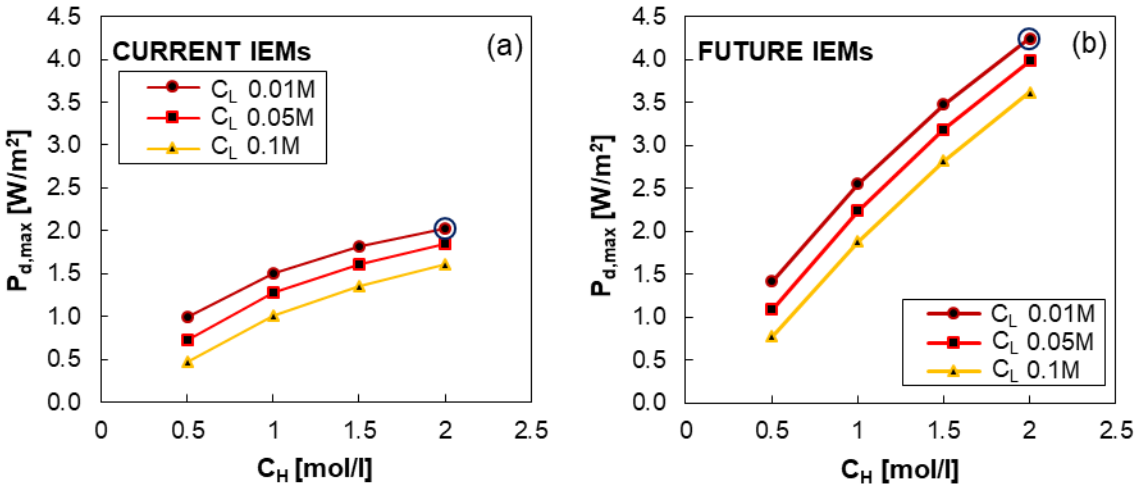

Figure 5. *Effect of inlet concentrations on $P_{d,max}$ of the RED unit for current (a) and future (b) scenarios. RED unit 1000 cell pairs 0.5x0.5 m^2, inlet velocities equal to 1 cm/s. Blue circle is used to highlight the best performance conditions.*

The effect of RED inlet concentration on the thermal power consumption of the vapour stripping column is reported in Figures 6a and 6b for current and future membranes, respectively. The higher the power generated in the RED unit, the higher is the salinity gradient consumed, and therefore, the higher the thermal power consumption of the stripping column. The lowest TPC values (around 160 kW) are obtained for the smaller salinity gradient considered (0.5 M-0.1 M). Similar thermal energy consumptions are obtained for the two scenarios, i.e., current and future (fig. 6), due to the effect of mixer 1. It should be observed that the two solutions exiting from the RED unit have different concentration values for the current and future scenarios, respectively. Conversely, the two solutions entering the regeneration unit have similar concentration values for the current and future scenarios, due to the partial mixing process required for the water-rebalancing.

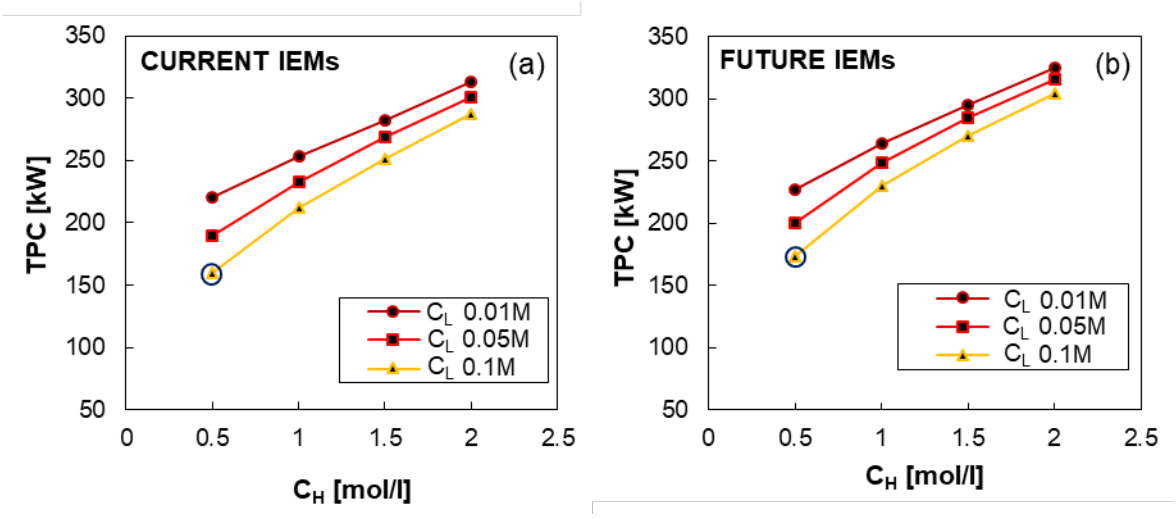

375

376 ***Figure 6.*** *Effect of inlet concentrations on TPC of the vapour stripping column for current (a) and*
377 *future (b) scenarios. RED unit 1000 cell pairs 0.5x0.5 m^2, inlet velocities equal to 1 cm/s. $T_{waste-heat}$=80 °C. Blue circle is used to highlight the conditions for the best performance.*

379

380 The ratio between the gross power output of the RED unit and the TPC of the regeneration unit
381 is the thermal efficiency. Figure 7 shows the effect of inlet concentration on the thermal and
382 exergy efficiencies for current (a) and future membranes (b). In both cases, the highest
383 efficiency is achieved for the highest driving force (2 M-0.01 M) because the salinity gradient
384 affects the power production more than TPC. As a matter of fact, considering the current
385 scenario and C_L=0.01 M, an increase of the concentration of the high solution from 0.5 M to 2
386 M doubles the power density from 1 W/m^2 to 2 W/m^2, while the thermal energy consumption
387 increases about 50%. This effect is more marked in the future scenario where the power density
388 is increased almost three times (i.e., from 1.5 W/m^2 to 4.25 W/m^2), while the power
389 consumption is comparable to the one in the current scenario. As result, the highest thermal
390 efficiency in the current scenario is equal to 0.16% (η_{ex}= 0.9%), while in the future scenario is
391 equal to 0.32% (η_{ex}= 1.93%).

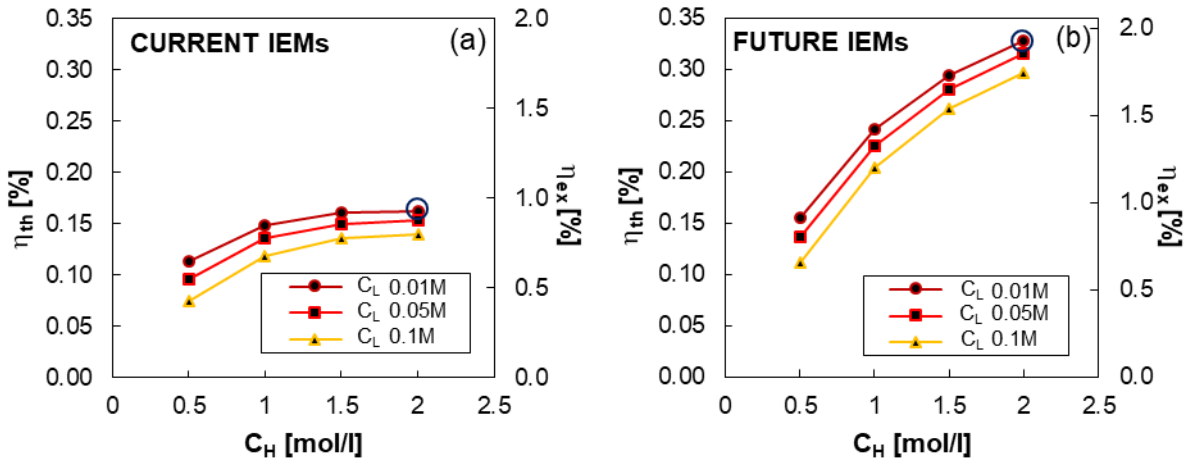

Figure 7*. Effect of the inlet concentrations on η_{th} and η_{ex} of the t-RED HE for current (a) and future (b) scenarios. RED unit 1000 cell pairs 0.5x0.5 m^2, inlet velocities equal to 1 cm/s. Blue circle is used to highlight the conditions of the best performance.*

3.2 Influence of inlet velocities on the system performance

The following sensitivity analyses concern the effect of the inlet solution velocities on the main performance parameters of the t-RED HE, fixing the inlet concentration of the two solutions in the RED unit to the values that provided the highest efficiency in the previous analysis (i.e., C_H=2 M and C_L=0.01 M).

The influence of the feed inlet velocities on $P_{d,max}$ is reported in Figure 8. As expected, the gross power density is a growing function of the solution velocities. In particular, $P_{d,max}$ is affected by the dilute velocity, while only slight variations are observed with the concentrate velocity. The highest $P_{d,max}$ is equal to 2.6 W/m^2 in the current scenario. Due to the membrane improvements, $P_{d,max}$ in the future scenario is more than double of the current one, i.e., 5.7 W/m^2.

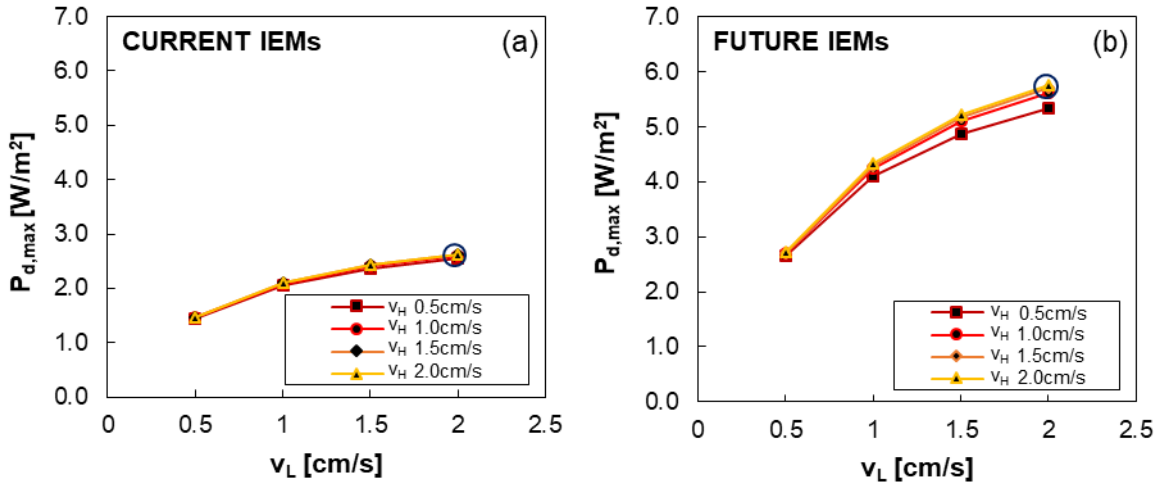

407

408 ***Figure 8.*** *Effect of the inlet velocities on $P_{d,max}$ of the RED unit for current (a) and future (b)*

409 *scenarios. RED unit 1000 cell pairs 0.5x0.5 m^2, inlet concentrations equal to C_H=2 M and C_L=0.01 M.*

410 *Blue circle is used to highlight the conditions of the best performance.*

411

412 The influence of RED inlet velocities on the TPC of the vapour stripping column is reported in

413 Figures 9a and 9b for current and future membranes, respectively. TPC linearly increases with

414 the dilute flow rate. The higher the dilute flow rate fed to the stripping column, the higher the

415 amount of stripping vapour that is required in the regeneration unit. TPC is slightly affected by

416 the velocity of the concentrate and the adoption of either current or future membranes. The

417 lowest TPC of about 180 kW is observed in the case of dilute inlet velocities of 0.5 cm/s.

418

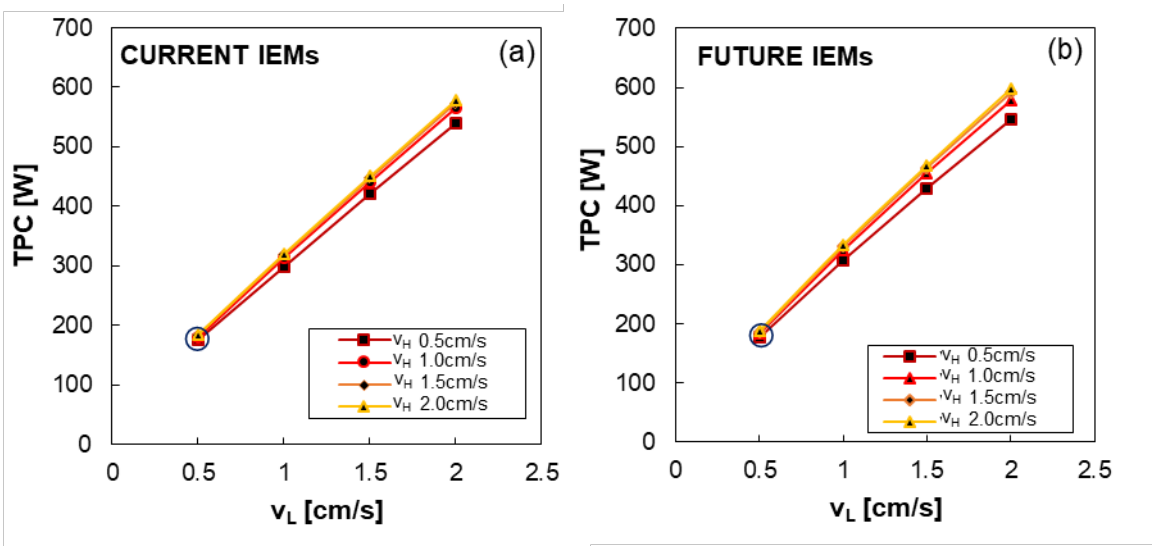

Figure 9. *Effect of the inlet velocities on TPC of the vapour stripping column for current (a) and future (b) scenarios. RED unit 1000 cell pairs 0.5x0.5m^2, inlet concentrations equal to C_H=2 M and C_L=0.01 M. $T_{waste\text{-}heat}$=80 °C. Blue circle is used to highlight the conditions of the best performance.*

The effect of RED inlet velocities on the thermal and exergy efficiencies of the whole t-RED HE is depicted in Figures 10a and 10b for current and future membranes, respectively. In both current and future scenarios, the efficiency of the unit is dominated by the influence of the velocities on TPC. Thus, the maximum efficiency is obtained for the lowest TPC, which is observed at the lowest inlet velocities (i.e., v_H=v_L= 0.5 cm/s). The highest thermal efficiency in the current scenario is equal to 0.2%, which corresponds to an exergy efficiency of 1.1%. In the case of future enhanced membranes, the thermal efficiency increases up to 0.36% while the exergy efficiency reaches values around 2.10%.

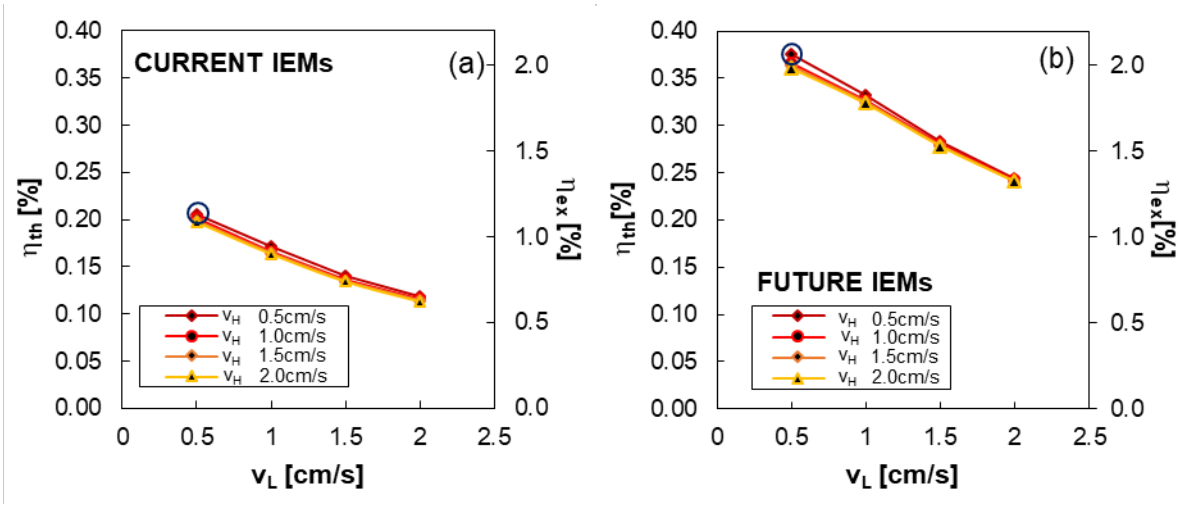

Figure 10. *Effect of inlet velocities on η_{th} and η_{ex} of the t-RED HE for current (a) and future (b) scenarios. RED unit 1000 cell pairs 0.5x0.5 m^2, inlet concentrations equal to C_H=2 M and C_L=0.01 M. Single. $T_{waste\text{-}heat}$=80 °C. Blue circle is used to highlight the conditions of the best performance.*

3.3 Multi-stage regeneration unit

The previous sensitivity analyses on the t-RED HE has highlighted that in all the investigated conditions, the high thermal consumption of the vapour stripping column is the limiting factor, which leads to low efficiency values also in the case of future enhanced membranes. The high thermal power consumption is caused by the partial vaporization of the solution in the reboiler to generate the stripping steam. However, only a small part of the thermal energy contained in this stream is used to strip the gas. As a result, most of the heat that is supplied remains in the vapour steam exiting from the top of the column and it is discharged in the condensation step (see condenser in *Figure 3*). In order to increase the energetic efficiency of the regeneration unit, this heat should be recovered and reused within the unit.

A possible alternative already proposed in the literature [30] for forward osmosis applications is to exploit the enthalpy of vaporization remaining in the stripping gas as an energy source for a following stripping column operating at lower pressure. In this way, a multi-column configuration is obtained, similarly to a MED unit. When a multi-column system is considered,

449 the solution exiting from mixer 1 (Figure 11) is split and fed in parallel to the stripping columns.
450 Only the heat supplied in the first column is coming from an external source (i.e., waste heat),
451 while the following columns are fed by the heat obtained from vapour condensation of the
452 previous column as shown in Figure 11. The absorption step operates in the same way for both
453 single and multi-stage processes as the amount of gases stripped in the two different
454 configurations remains practically the same.
455 Differently from the MED process, where a large number of effects can be adopted to increase
456 the thermal efficiency of the process, in the present case of a multi-column arrangement, the
457 number of columns or stages is limited due to the multi-component nature of the condensing
458 vapour. Indeed, the condensation process takes place not at constant temperature but in a range
459 of condensation temperatures between 4-8 °C, consuming rapidly the available temperature
460 difference between the first and the last columns, and resulting in a small number of units. As
461 an example, fixing the top temperature at 80 °C and the lowest operating pressure equal to 0.05
462 bar (i.e. bottom temperature around 30 °C), the maximum number of columns is equal to 5.

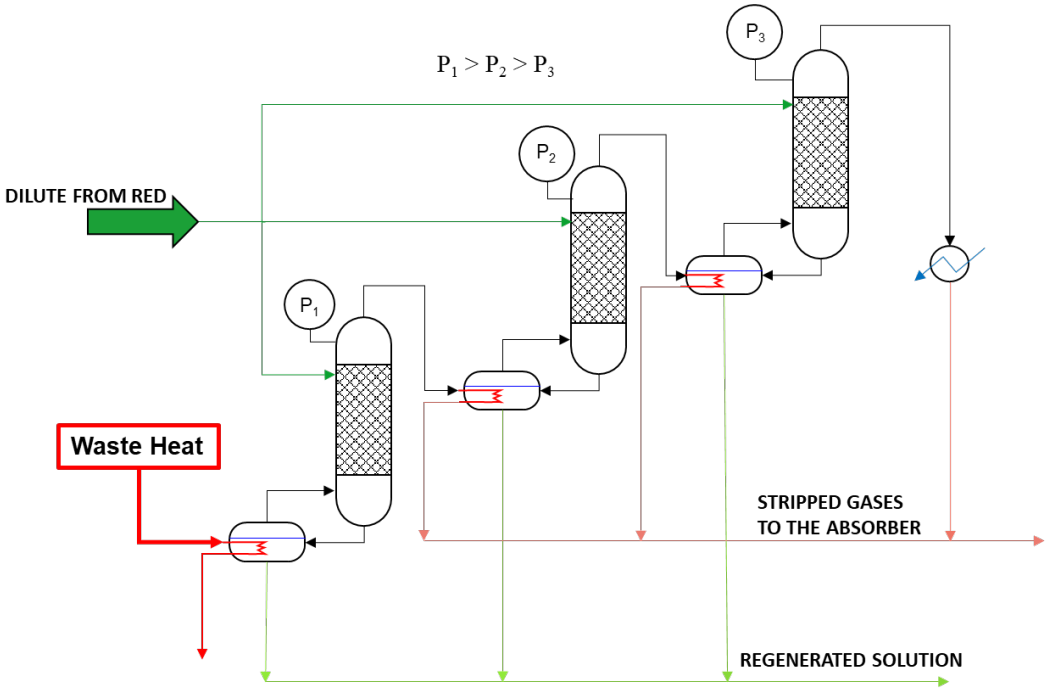

463

464 ***Figure 11.*** *Schematic representation of a three stages vapour stripping column.*

465

The thermal and exergy efficiencies of the t-RED HE fed by waste heat at 80°C as a function of the number of columns in series, are reported in Figure 12. Operating conditions at the RED unit inlet (i.e., concentration and velocity of solutions) were fixed equal to those of the previous sections 3.1 and 3.2, which led to the highest efficiency (i.e., C_H = 2 M C_L = 0.01 M v_H = v_L= 0.5 cm/s). The efficiency increase is not a linear function of the number of stripping columns. In fact, the efficiency is more than doubled when shifting from 1 to 2 columns (from $\eta_{ex,1}$ = 1.3% to $\eta_{ex,2}$ =2.7%), while it is only four times higher in the case of 5 columns in series ($\eta_{ex,5}$=5.1%). In the future scenario, using a 5-column configuration the thermal and exergy efficiencies are equal to 1.4% and 8.5%, respectively.

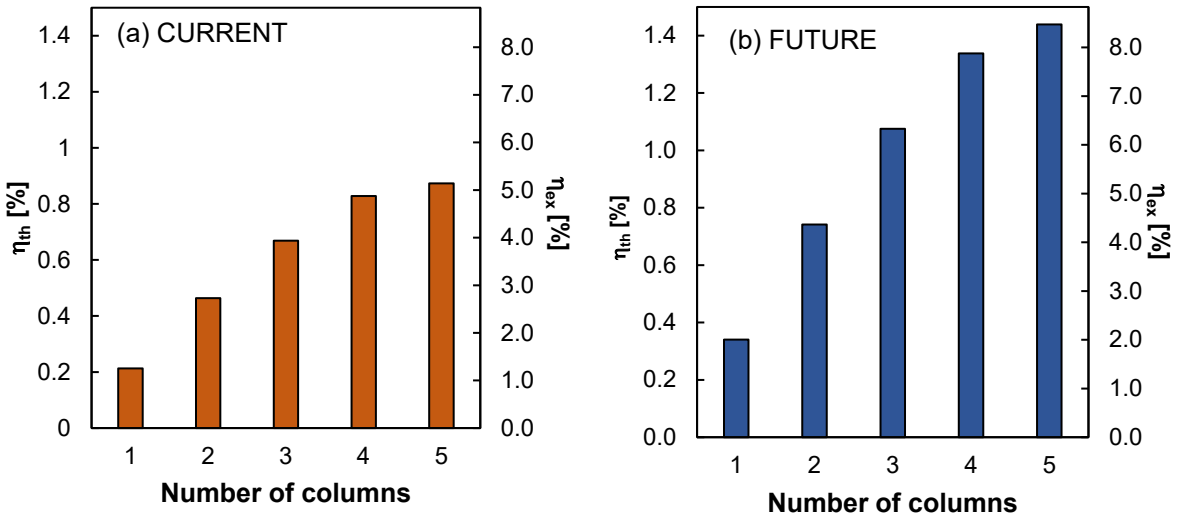

Figure 12. *Thermal and exergy efficiencies of the t-RED HE as a function of the number of stripping column adopted in the regeneration unit for current (a) and future (b) membranes. RED unit 1000 cell pairs 0.5x0.5 m^2, v_H= v_L=0.5 cm/s, C_H=2 M, C_L=0.01 M. $T_{waste-heat}$=80 °C, $T_{last,column}$=30 °C.*

Interestingly, the temperature of the waste heat fed into the first reboiler determines the number of stripping units placed in series. The lower the waste heat temperature, the less stripping columns can be used and thus the lower the thermal efficiency. In this work, the temperature of waste heat was fixed at 80 °C, as any further temperature increase has been proven to generate a negligible efficiency increase of the multi-column system. However, the increase of waste

heat temperature can be useful to increase the temperature driving force for heat exchange in the reboilers, thus reducing the heat exchanger area and the relevant capital cost.

4 CONCLUSIONS

In this work, an experimentally validated model was developed to analyse the performance of the t-RED HE varying the operating conditions and considering (i) a current scenario where commercial membranes (i.e., Fujifilm Type 10 membranes) are used and (ii) a future scenario where enhanced membrane properties are adopted. The highest exergy efficiency achieved in the current scenario is equal to 1.25% while in the future scenario it is equal to ~2%.

Higher efficiencies can be reached by adopting a multi-stage regeneration unit due to the increase of the thermal efficiency of the regeneration, achieving a better exploitation of the external waste heat. The exergy efficiency of the system is increased from 1.25% to 5.2% when using 5 columns. A further increase up to 8.5% is obtainable considering enhanced future membranes.

This novel heat engine converts very low-grade heat (e.g. below 100°C) into power. However, the efficiencies found are low thus suggesting the need for further improvements. The use of alternative solvent-solute couples or even the adoption of salt mixtures should be investigated in the future, in order to find more efficient solutions.

Achieving higher efficiency values at acceptable costs would guarantee the recovery of large amounts of waste heat available at low temperature levels which the RED HE is able to convert. This would allow industrial power plants to increase their efficiency and sustainability by reducing the energy costs and the carbon dioxide emissions.

ACKNOWLEDGEMENTS

This work was performed within the RED-Heat-to-Power project (Conversion of Low-Grade Heat to Power through closed loop Reverse Electro-Dialysis), funded by EU within the H2020 Research & Innovation Programme, Grant Agreement No. 640667 [31].

NOMENCLATURE

A_{cp}	cell pair membrane area (m^2)
b	membrane width (m)
C_H	concentrate molar concentration (M)
C_L	dilute molar concentration (M)
E_{cell}	voltage generated by the cell pair (V)
E_{stack}	voltage generated by the pile (V)
F	Faraday constant (C/mol)
$i(k)$	electric current of the generic k^{th} element
I_{stack}	total Electric current (A)
m	molality (mol/kg_{solv})
$M1$	mixer 1
$M2$	mixer 2
MW_s	salt Molecular weight (kg/mol)
N_{cp}	number of cell pair
N_k	number of discretization elements
P_d	power density (W/m^2)
$P_{d,max}$	maximum power density (W/m^2)
P_{loss}	pumping power required (W)
P_{RED}	electric power outputs from the RED unit (W)
Q	volumetric flowrate (m^3/s)
R	universal gas constant (J/(K mol))
R_{AEM}	anionic membrane resistance (Ωm^2)
R_{blamk}	electrical resistance of the electrodic compartment (Ω)
R_{cell}	electrical resistance of the cell pair (Ω)

R_{CEM}	cationic membrane resistance (Ωm^2)
R_E	load resistance (Ω)
R_H	electrical resistance of concentrate (Ωm^2)
$R_{IEM,av}$	average ionic exchange membrane resistance (Ωm^2)
R_L	electrical resistance of dilute (Ωm^2)
T	temperature (°C or K)
TPC	thermal power consumption (W)
v	solution velocity (m/s)
z	valence of the ions

Greek symbols

α_{av}	average ionic exchange membrane permselectivity
Δx	calculation element length (m)
η_C	Carnot efficiency
η_{ex}	exergy efficiency
η_{th}	thermal efficiency
γ	salt activity coefficient (dimensionless)
ρ	density (kg/m^3)

Subscripts

gross	related to gross value
H	related to the concentrate stream
H-mix1	related to the part of the outlet concentration fed to the mix1
in	related to the inlet solution from RED unit
L	related to the dilute stream
mix1	related to the outlet solution from mixer 1
net	related to net consumptions
out	related to the outlet solution from RED unit
HOT	related to the hot reservoir
COLD	related to the cold reservoir
waste-heat	related to the waste heat

Acronyms

E-NRTL-RK	Electrolyte Non Random Two Liquid Redlich-Kwong
HE	Heat Engine
IEM	Ionic Exchange Membrane
MD	Membrane Distillation
MED	Multi Effect Distillation
PRO	Pressure Retarded Osmosis
PRO-MD HE	Pressure Retarded Osmosis Membrane Distillation Heat Engines
RED	Reverse Electrodialysis
RED HE	Reverse ElectroDialysis Heat Engine
SGP	Salinity Gradient Power
SGP HE	Salinity Gradient Power Heat Engines
t-RED HE	Thermolytic Reverse ElectroDialysis Heat Engine

REFERENCES

[1] A. Tamburini, M. Tedesco, A. Cipollina, G. Micale, M. Ciofalo, M. Papapetrou, W. Van Baak, A. Piacentino, Reverse electrodialysis heat engine for sustainable power production, Appl. Energy. 206 (2017) 1334–1353. doi:10.1016/j.apenergy.2017.10.008.

[2] M. Papapetrou, G. Kosmadakis, A. Cipollina, U. LaCommare, G. Micalea, Industrial waste heat: Estimation of the technically available resource in the EU per industrial sector, temperature level and country, Appl. Therm. Eng. 138 (2018) 207–216. doi:10.1016/j.applthermaleng.2018.04.043.

[3] B.E. Logan, M. Elimelech, Membrane-based processes for sustainable power generation using water, Nature. 488 (2012) 313–319. doi:10.1038/nature11477.

[4] S. Loeb, Method and apparatus for generating power utilizing Pressure-Retarded-Osmosis, US Patent 3906250, 1974.

[5] S. Loeb, Method and apparatus for generating power utilizing Reverse Electrodialysis, US Patent 4171409, 1978.

[6] S. Lin, N.Y. Yip, T.Y. Cath, C.O. Osuji, M. Elimelech, Hybrid Pressure Retarded Osmosis–

Membrane Distillation System for Power Generation from Low-Grade Heat: Thermodynamic Analysis and Energy Efficiency, Environ. Sci. Technol. 48 (2014) 5306–5313. doi:10.1021/es405173b.

[7] R. Long, B. Li, Z. Liu, W. Liu, Hybrid membrane distillation-reverse electrodialysis electricity generation system to harvest low-grade thermal energy, J. Memb. Sci. 525 (2017) 107–115. doi:10.1016/j.memsci.2016.10.035.

[8] M. Micari, A. Cipollina, F. Giacalone, G. Kosmadakis, M. Papapetrou, G. Zaragoza, G. Micale, A. Tamburini, Towards the first proof of the concept of a Reverse ElectroDialysis - Membrane Distillation Heat Engine, Desalination. 453 (2019) 77–88. doi:10.1016/j.desal.2018.11.022.

[9] J. Hu, S. Xu, X. Wu, D. Wu, D. Jin, P. Wang, Q. Leng, Theoretical simulation and evaluation for the performance of the hybrid multi-e ff ect distillation — reverse electrodialysis power generation system, 443 (2018) 172–183. doi:10.1016/j.desal.2018.06.001.

[10] P. Palenzuela, M. Micari, B. Ortega-Delgado, F. Giacalone, G. Zaragoza, D.-C. Alarcón-Padilla, A. Cipollina, A. Tamburini, G. Micale, Performance Analysis of a RED-MED Salinity Gradient Heat Engine, Energies. 11 (2018) 3385. doi:10.3390/en11123385.

[11] E. Shaulsky, C. Boo, S. Lin, M. Elimelech, Membrane-based osmotic heat engine with organic solvent for enhanced power generation from low-grade heat, Environ. Sci. Technol. 49 (2015) 5820–5827. doi:10.1021/es506347j.

[12] M. Marino, L. Misuri, A. Carati, D. Brogioli, Proof-of-concept of a zinc-silver battery for the extraction of energy from a concentration difference, Energies. 7 (2014) 3664–3683. doi:10.3390/en7063664.

[13] K.L. Hickenbottom, J. Vanneste, T.Y. Cath, Assessment of alternative draw solutions for optimized performance of a closed-loop osmotic heat engine, J. Memb. Sci. 504 (2016) 162–175. doi:10.1016/j.memsci.2016.01.001.

[14] A. Carati, M. Marino, D. Brogioli, Thermodynamic study of a distiller-electrochemical cell system for energy production from low temperature heat sources, Energy. 93 (2015) 984–993. doi:10.1016/j.energy.2015.09.108.

[15] F. Giacalone, C. Olkis, G. Santori, A. Cipollina, S. Brandani, G. Micale, Novel solutions for

555 closed-loop reverse electrodialysis: Thermodynamic characterisation and perspective analysis,
556 Energy. 166 (2019) 674–689. doi:10.1016/j.energy.2018.10.049.
557 [16] M. Micari, M. Bevacqua, A. Cipollina, A. Tamburini, W. Van Baak, T. Putts, G. Micale, Effect
558 of different aqueous solutions of pure salts and salt mixtures in reverse electrodialysis systems
559 for closed-loop applications, J. Memb. Sci. 551 (2018) 315–325.
560 doi:10.1016/j.memsci.2018.01.036.
561 [17] R.L. McGinnis, J.R. McCutcheon, M. Elimelech, A novel ammonia–carbon dioxide osmotic heat
562 engine for power generation, J. Memb. Sci. 305 (2007) 13–19.
563 doi:10.1016/j.memsci.2007.08.027.
564 [18] X. Luo, X. Cao, Y. Mo, K. Xiao, X. Zhang, P. Liang, X. Huang, Power generation by coupling
565 reverse electrodialysis and ammonium bicarbonate: Implication for recovery of waste heat,
566 Electrochem. Commun. 19 (2012) 25–28. doi:10.1016/j.elecom.2012.03.004.
567 [19] R.D. Cusick, Y. Kim, B.E. Logan, Energy Capture from Thermolytic Solutions in Microbial
568 Reverse-Electrodialysis Cells, Science (80-.). 335 (2012) 1474–1477.
569 doi:10.1126/science.1219330.
570 [20] K. Kwon, B.H. Park, D.H. Kim, D. Kim, Parametric study of reverse electrodialysis using
571 ammonium bicarbonate solution for low-grade waste heat recovery, Energy Convers. Manag.
572 103 (2015) 104–110. doi:10.1016/j.enconman.2015.06.051.
573 [21] M. Bevacqua, A. Carubia, A. Cipollina, A. Tamburini, M. Tedesco, G. Micale, Performance of
574 a RED system with ammonium hydrogen carbonate solutions, Desalin. Water Treat. 57 (2016)
575 23007–23018. doi:10.1080/19443994.2015.1126410.
576 [22] D.H. Kim, B.H. Park, K. Kwon, L. Li, D. Kim, Modeling of power generation with thermolytic
577 reverse electrodialysis for low-grade waste heat recovery, Appl. Energy. 189 (2017) 201–210.
578 doi:10.1016/j.apenergy.2016.10.060.
579 [23] M. Bevacqua, A. Tamburini, M. Papapetrou, A. Cipollina, G. Micale, A. Piacentino, Reverse
580 electrodialysis with NH4HCO3-water systems for heat-to-power conversion, Energy. 137 (2017)
581 1293–1307. doi:10.1016/j.energy.2017.07.012.
582 [24] F. Giacalone, P. Catrini, A. Tamburini, A. Cipollina, A. Piacentino, G. Micale, Exergy analysis

of reverse electrodialysis, Energy Convers. Manag. 164 (2018) 588–602. doi:10.1016/j.enconman.2018.03.014.

[25] T.Z. Fahidy, Activity coefficients in electrolyte solutions (second edition), edited by Kenneth S. Pitzer, 1991, 542 + vi pages, CRC Press, Boca Raton, FL; ISBN 0-8493-5415-3. Price: US$ 195.00, Can. J. Chem. Eng. 71 (1993) 494–494. doi:10.1002/cjce.5450710328.

[26] E.I. Rashkovskaya, E.A.; Chernen'kaya, Densities of ammonium bicarbonate, sodium bicarbonate, and ammonium chloride and ammonia salt solutions at 20-100°C, Zhurnal Prikl. Khimii. 40 (1967) 301.

[27] G. Jones, C.F. Bickford, The Conductance of Aqueous Solutions as a Function of the Concentration. I. Potassium Bromide and Lanthanum Chloride, J. Am. Chem. Soc. 56 (1934) 602–611. doi:10.1021/ja01318a021.

[28] R. Ashu, S. Pawlowski, J. Veerman, K. Bouzek, E. Fontananova, S. Velizarov, J. Goulão, K. Nijmeijer, E. Curcio, Progress and prospects in reverse electrodialysis for salinity gradient energy conversion and storage, 225 (2018) 290–331. doi:10.1016/j.apenergy.2018.04.111.

[29] A. Tamburini, A. Cipollina, M. Papapetrou, A. Piacentino, G. Micale, 7 – Salinity gradient engines, in: Sustain. Energy from Salin. Gradients, 2016: pp. 219–256. doi:10.1016/B978-0-08-100312-1.00007-9.

[30] R.L. McGinnis, M. Elimelech, Energy requirements of ammonia–carbon dioxide forward osmosis desalination, Desalination. 207 (2007) 370–382. doi:10.1016/j.desal.2006.08.012.

[31] EU, RED-Heat-to-Power, (2015). www.red-heat-to-power.eu. (accessed February 22, 2019).

[32] T.Z. Fahidy, Activity coefficients in electrolyte solutions (second edition), edited by Kenneth S. Pitzer, 1991, 542 + vi pages, CRC Press, Boca Raton, FL; ISBN 0-8493-5415-3. Price: US$ 195.00, Can. J. Chem. Eng. 71 (1993) 494–494. doi:10.1002/cjce.5450710328.

[33] Z. Meng, J.H. Seinfeld, P. Saxena, Y.P. Kim, Atmospheric Gas-Aerosol Equilibrium: IV. Thermodynamics of Carbonates, Aerosol Sci. Technol. 23 (1995) 131–154. doi:10.1080/02786829508965300.

APPENDIX

A.1. Ammonium bicarbonate-water solution properties

Osmotic and mean activity coefficients of ammonium bicarbonate-water solutions

Pitzer's ion interaction model [32] was used to evaluate the osmotic and activity coefficients of NH_4HCO_3-water solutions. In Pitzer's equation the osmotic and mean activity coefficients are expressed as function of the solution molality through fitting coefficients, named virial coefficients, which account for the interactions between the ions.

$$\varphi = 1 - \left|z_M z_X\right| A_\varphi \frac{I^{0.5}}{1 + bI^{0.5}} + 2m\frac{\nu_M \nu_X}{\nu} B^{\varphi}_{MX} + 2m^2 \frac{(\nu_M \nu_X)^{3/2}}{\nu} C^{\varphi}_{MX} \quad \text{(A.1)}$$

$$\ln(\gamma_{\pm}) = -\left|z_M z_X\right| A_\varphi \left(\frac{I^{0.5}}{1 + bI^{0.5}} + \frac{2}{b}\ln(1 + bI^{0.5}) \right) + 2m\frac{\nu_M \nu_X}{\nu} B^{\gamma}_{MX} + 3m^2 \frac{(\nu_M \nu_X)^{3/2}}{\nu} C^{\varphi}_{MX} \quad \text{(A2)}$$

With

$$B^{\varphi}_{MX} = B^{(o)}_{MX} + B^{(1)}_{MX} \exp(-\alpha I^{0.5}) \quad \text{(A.3)}$$

$$B^{\gamma}_{MX} = 2B^{(o)}_{MX} + \frac{2B^{(1)}_{MX}}{\alpha^2 I}\left[1 - (1 + \alpha I^{0.5} - \frac{\alpha^2 I}{2}) \exp(-\alpha I^{0.5}) \right] \quad \text{(A.4)}$$

where $m_0 = 1$ mol·kg^{-1} is the standard molality, $b = 1.2$ kg$^{1/2}$mol$^{-1/2}$ is a universal parameter; α is a numerical constant equal to 2 for univalent ions; I is the ionic strength A_ϕ, is the Debye-Huckel parameter for the osmotic coefficient; z_M and z_X are the charges of cation and anion; $B^{(0)}_{MX}$, $B^{(1)}_{MX}$, and C_{MX} are the *ion-interaction parameters or virial coefficients*. The virial coefficients for NH_4HCO_3 solutions at 298°K are reported in [33]. The behaviour of osmotic and activity coefficients as function of solution molality at 298°K is reported in Figure A. 1.

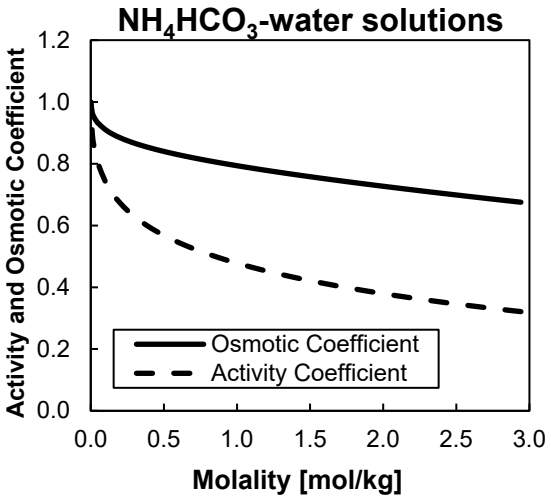

Figure A. 1. *Osmotic and salt activity coefficients for NH_4HCO_3-water solution at 298.15 K as function of molality. Pitzer's coefficients from* [33].

Density of ammonium bicarbonate-water solutions

The NH_4HCO_3-water density was evaluated as a linear function of the molar concentration as:

$$\rho = \rho_0 + \left(\frac{\Delta\rho}{\Delta C}\right) C \tag{A.5}$$

where ρ_0 is density of pure water at 298.15 K, which is equal to 997 kg/m^3. The slope of the function $(\Delta\rho/\Delta C)$ was evaluated by fitting experimental data from literature [26]. In the case of NH_4HCO_3-water solution, $\Delta\rho/\Delta C$ is equal to 35.53 kg/mol. Figure A. 2a shows the density of NH_4HCO_3-water solution as function of the molar concentration. As it can be seen a good fitting was found.

Conductivity of ammonium bicarbonate-water solutions

The conductivity of NH_4HCO_3-water solutions as function of solution molarity is computed according to Eq. A.6 [27].

$$\Lambda = \Lambda_0 - \frac{A_\Lambda C^{1/2}}{1 + B_\Lambda C^{1/2}} - C_\Lambda C \tag{A.6}$$

where Λ_0 is the equivalent conductivity of salt at infinite dilution, A_Λ, B_Λ and C_Λ are fitting parameters, and C is the molar concentration. The parameters of equation A.6 for NH_4HCO_3-water solutions, obtained by fitting of experimental data are $A_\Lambda=30.32$, $B_\Lambda=0$ and $C_\Lambda=0$. The

646 dependence of conductivity on the concentration for NH_4HCO_3 aqueous solutions is reported
647 in Figure A.2b, where the soundness of the correlation can be also observed.

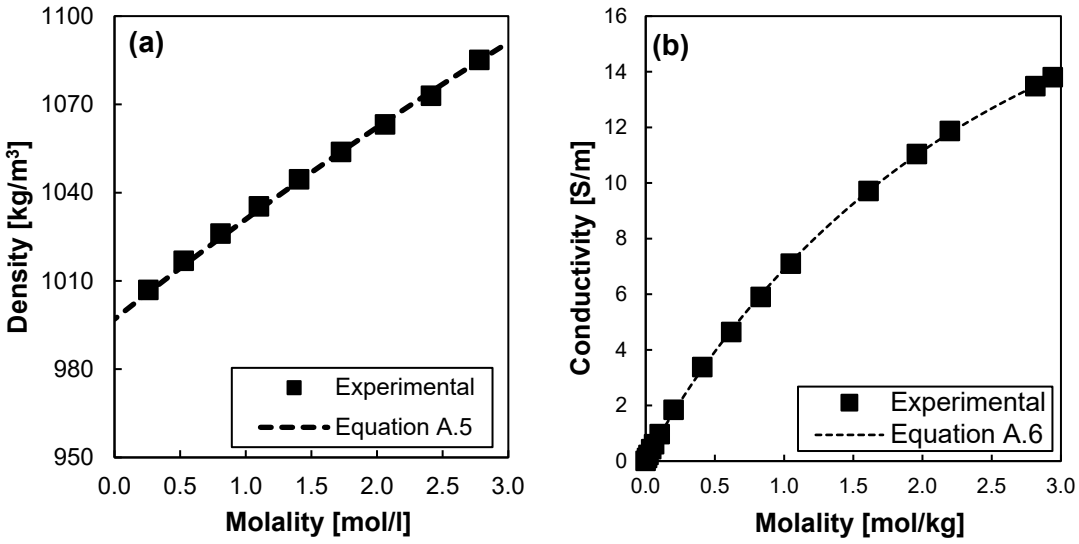

648

649 **Figure A.2.** *Comparison of experimental and fitting results of density (a) and conductivity (b) for*
650 *NH_4HCO_3 aqueous solutions as function of molarity at 298.15 K.*

651